PROCEEDINGS OF SCIENCE

Resuts of the Heavy Cosmic-Ray Analysis with CALET on the International Space Station

Caterina Checchia[a,b,*] **for the CALET collaboration**

[a] *Department of Physical Sciences, Earth and Environment, University of Siena, via Roma, 56, 53100 Siena, Italy*

[b] *INFN Sezione di Pisa, Polo Fibonacci, Largo B. Pontecorvo, 3, 56127 Pisa, Italy*

E-mail: caterina.checchia2@unisi.it

The study of the spectral behavior of charged cosmic-ray elements is of particular interest to gain a deeper understanding of propagation and acceleration phenomena in our Galaxy. The Calorimetric Electron Telescope (CALET), launched to the International Space Station in 2015, provides more than 7 years of continuous observation of high energy cosmic rays up to ~1 PeV. CALET can measure cosmic-ray charge up to Z = 40 and, with its 27 radiation lengths deep Total Absorption Calorimeter, it measures particle energy, allowing for the determination of spectra up to nickel. In this contribution we present a direct measurement of several charged nuclei spectra from boron to nickel, including the boron to carbon and the nickel to iron ratios. Also, the ultra heavy nuclei analysis results are reported.

Multifrequency Behaviour of High Energy Cosmic Sources XIV (MULTIF2023)
12-17 June 2023
Palermo, Italy

*Speaker

PoS(MULTIF2023)011

1. Introduction

CALET is a space experiment aboard the International Space Station (ISS), designed for long-term observations of charged and neutral cosmic radiation [1]. The instrument is managed by an international collaboration led by the Japanese Space Agency (JAXA) with the participation of the Italian Space Agency (ASI) and NASA. It was launched on August 19, 2015 with the Japanese carrier H-IIB, delivered to the ISS by the HTV-5 Transfer Vehicle, and installed on the Japanese Experiment Module Exposure Facility (JEM-EF). The science program of CALET addresses several outstanding questions of high-energy astroparticle physics including the origin of cosmic rays (CR), the possible presence of nearby astrophysical CR sources, the acceleration and propagation of primary and secondary elements in the galaxy, and the nature of dark matter. Although the design of CALET is optimised for high precision measurements of the electron+positron spectrum with an accurate scan of the energy interval already covered by previous experiments and its extension to the region above 1 TeV, it can identify cosmic rays with individual element resolution, carrying out direct measurements of the spectra and relative abundances of light and heavy cosmic nuclei [2–7], from proton to nickel, in the energy interval from $\sim$ 50 GeV (for the lighter nuclei, 10 GeV/n for the heavier) to several hundred TeV. The abundances of trans-iron elements up to Z $\sim$ 40 are studied with a dedicated program of long term observations [8].

2. The CALET detector

CALET is based on a thick calorimetric instrument (30 radiation lengths), designed to achieve electromagnetic shower containment and a large proton rejection capability (>10^5). It is longitudinally segmented into a fine grained imaging calorimeter (IMC) followed by a total absorption calorimeter (TASC). The TASC is a 27 X_0 thick homogeneous calorimeter with 12 alternate X-Y layers of lead-tungstate (PWO) logs. The IMC is a sampling calorimeter longitudinally segmented into 16 layers of scintillating fibers (with 1 mm^2 square cross-section), readout individually, and interspaced with thin tungsten absorbers. Alternate planes of fibers are arranged along orthogonal directions. It can image the early shower profile in the first 3 X_0 and reconstruct the incident direction of cosmic rays with good angular resolution (0.1° for electrons and better than 0.5° for hadrons) [9]. The overall thickness of CALET at normal incidence is ~1.3 proton interaction lengths (λ_I). The charge identification of individual nuclear species is performed by a two-layered hodoscope of plastic scintillators (CHD), positioned at the top of the apparatus, providing a measurement of the charge Z of the incident particle over a wide dynamic range (Z = 1 to $\sim$ 40) with sufficient charge resolution to resolve individual elements [10] and complemented by a redundant charge determination via multiple dE/dx measurements in the IMC. The overall CHD charge resolution (in Z units) increases linearly, as a function of the atomic number, from < 0.1 for protons to ~0.3 for iron. For the IMC, although the photostatistics available for a single fiber is about one order of magnitude lower than in the case of a single CHD layer, the charge measurement – thanks to the multiple sampling – achieves an excellent performance. The interaction point (IP) is first reconstructed [11] and only the dE/dx ionization clusters from the layers upstream the IP are used to infer a charge value from the truncated mean of the valid samples. The geometrical factor of

CALET is ~ 0.1 m^2sr and the total weight is 613 kg. The instrument is described in more detail elsewhere [12, 13].

3. Flight Operations and Calibrations

The commissioning of CALET aboard the ISS was successfully completed at the beginning of October 2015. Since then the instrument has been taking science data continuously with no major interruptions [14]. The on-orbit operations are controlled via the JAXA Ground Support Equipment (JAXA-GSE) in Tsukuba by the Waseda CALET Operations Center (WCOC) at Waseda University, Tokyo. As of February 28, 2023 a total observation time of more than 2696 days was integrated with a live time fraction ~86% of the total time, and ~3.9 billion events were collected above 1 GeV. An exposure of ~235 m^2 sr day was achieved with the high-energy (HE) trigger mode, designed to maximize the collection power for electrons above 10 GeV and other high-energy shower events. Energy calibrations of each channel of CHD, IMC, and TASC are performed with penetrating proton and He particles selected in-flight by a dedicated trigger mode. Raw signals are corrected for light output non-uniformity, gain differences among the channels, position and temperature dependence, as well as temporal gain variations [12, 15]. The four gain ranges of each TASC channel are calibrated with flight data and linked together to provide a seamless response spanning more than six orders of magnitude and allowing observations from one minimum ionizing particle to PeV showers.

4. Direct measurements of heavy cosmic ray nuclei

The energy spectrum of cosmic ray nuclei is obtained after an accurate selection of events: high energy trigger events are considered for all nuclei spectra. An additional off-line trigger confirmation is applied for B, C and O applying an higher threshold with respect than the onboard trigger. Since the trigger is fully efficient for Fe and Ni an offline trigger confirmation is not necessary for these nuclei because the HE trigger threshold is far below the signal amplitude expected from an ion at minimum ionization (MI). However, in order to select interacting particles, a deposit larger than 2 standard deviations of the MI peak is required in at least one of the first four layers of the TASC. A combinatorial Kalman filter algorithm is used to reconstruct the particle trajectory [16]: only events with a good reconstructed track are selected for the flux. Also, the trajectory of incident particles defines the acceptance: only events crossing the instrument from top of CHD to bottom of TASC (clear from the edge of TASC by 2 cm) are considered. At last, the charge selection is applied after requesting a consistency of the charge reconstructed from the two layers of CHD and the IMC for C, O and B. For Fe and Ni only the CHD can be used to reconstruct the charge (and to request the consistency) because of the saturation occurring in the IMC fibers for ions heavier than silicon. For B, C and O the events entering the detector from the lateral sides are rejected from the final sample through a dedicated selection [3]. In order to take into account the limited calorimetric energy resolution for hadrons (of the order of ~30%) an energy unfolding algorithm based on a Bayesian approach, is applied to correct for bin-to-bin migration effects. The flux of each nuclear specie is defined as

$$\Phi(E) = \frac{N(E)}{\epsilon(E)\Delta E S \Omega T} \tag{1}$$

$$N(E) = U[N_{obs}(E_{TASC}) - N_{bg}(E_{TASC})] \tag{2}$$

where $\epsilon(E)$ is the total efficiency, ΔE is the bin width, $S\Omega$ is the geometrical factor, T is the total live time, U is the unfolding operator, $N_{obs}(E_{TASC})$ is the number of observed events in each energy bin of deposited energy E_{TASC} and $N_{bg}(E_{TASC})$ is the number of contaminating events.

4.1 Carbon and Oxygen fluxes

The spectra of cosmic-ray carbon and oxygen and their ratio were published by CALET in [3]. They are shown in Fig. 1 in the energy range from 10 GeV/n to 2.2 TeV/n where uncertainties, including statistical and systematic errors, are represented by a gray band. CALET carbon spectrum is consistent with PAMELA [25] and with most previous experiments [17–23]. No oxygen spectrum was published by PAMELA. AMS-02 carbon and oxygen spectra [24] differ in the absolute normalization, which is lower for CALET by about 27% for both C and O. However they have very similar shapes as confirmed by the good consistency of the respective measurements of the C/O flux ratio. Fig. 2 shows the fits to CALET carbon and oxygen data (blue solid line) with a Double Power-Law (DPL) function

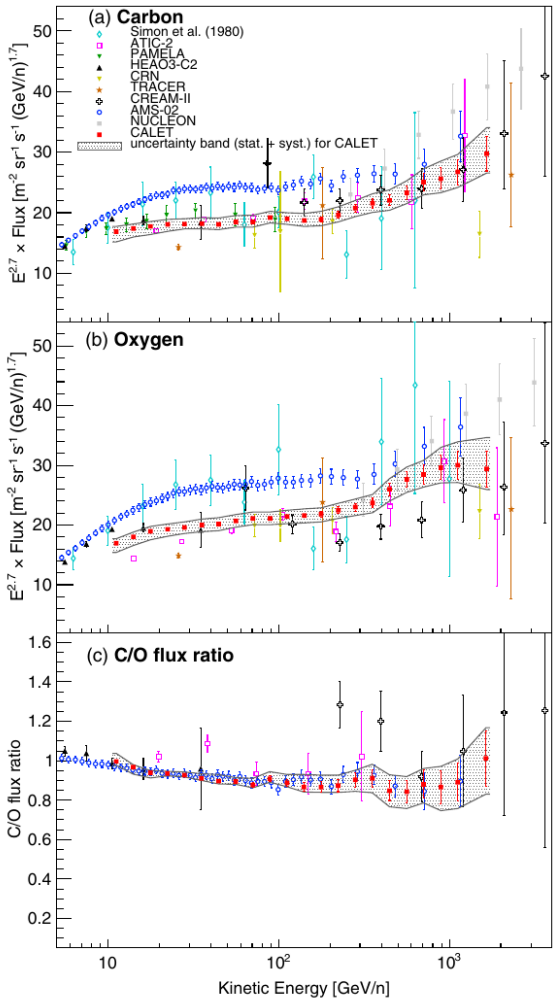

Figure 1: CALET (a) carbon and (b) oxygen flux (multiplied by $E^{2.7}$) and (c) ratio of carbon to oxygen fluxes, as a function of kinetic energy E. Error bars of CALET data (red) represent the statistical uncertainty only, while the gray band indicates the quadratic sum of statistical and systematic errors. Other direct measurements [17–25] are also plotted.

$$\Phi(E) \begin{cases} C\left(\frac{E}{\mathrm{GeV}}\right)^{\gamma} & \text{if } E \le E_0 \\ C\left(\frac{E}{\mathrm{GeV}}\right)^{\gamma}\left(\frac{E}{E_0}\right)^{\Delta\gamma} & \text{if } E > E_0 \end{cases} \tag{3}$$

where C is a normalization factor, γ the spectral index, and $\Delta\gamma$ the spectral index change above the transition energy E_0. A single power-law (SPL) function (Eq. 3 with $\Delta\gamma = 0$), fitted to the data in the energy range [25, 200] GeV/n and extrapolated above 200 GeV/n, is also shown for comparison (dashed line). The effect of systematic uncertainties in the measurement of the energy spectrum is modeled in the χ^2 minimization function with a set of 6 nuisance parameters [3]. The DPL fit to the C spectrum yields a spectral index $\gamma_C = -2.663 \pm 0.014$ at energies below the transition region $E_0^C = (215 \pm 54)$ GeV/n and a spectral index increase $\Delta\gamma_C = 0.166 \pm 0.042$ above, with χ^2/d.o.f. = 9.0/8.

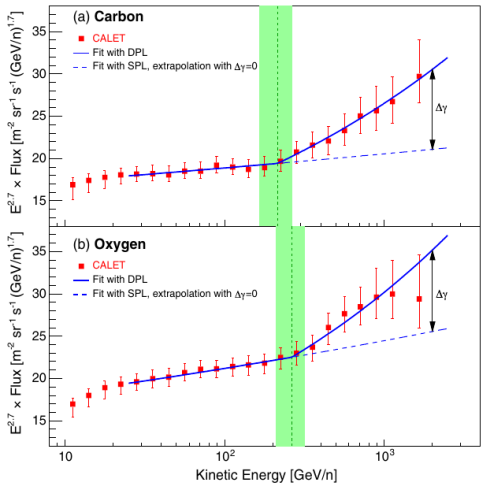

Figure 2: Fit of the CALET (a) C and (b) O energy spectra with a DPL function (blue line) in the energy range [25, 2000] GeV/n. The flux is multiplied by $E^{2.7}$ where E is the kinetic energy per nucleon. Error bars of CALET data points represent the sum in quadrature of statistical and systematic uncertainties. The dashed blue lines represent the extrapolation of a SPL function fitted to data in the energy range [25, 200] GeV/n. $\Delta\gamma$ is the change of the spectral index above the transition energy E_0, represented by the vertical green dashed line. The error interval for E_0 from the DPL fit is shown by the green band.

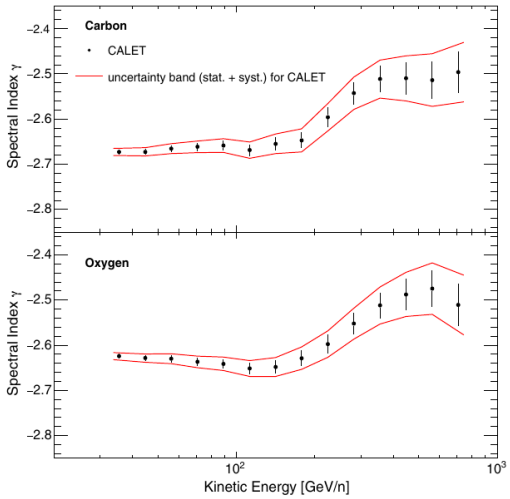

Figure 3: Energy dependence of the spectral index calculated within a sliding energy window for CALET (a) C and (b) O data. The spectral index is determined for each bin by fitting the data using ±3 bins. Red curves indicate the uncertainty range including systematic errors.

For oxygen, the fit yields $\gamma_O = -2.637 \pm 0.009$, $E_0^O = (264 \pm 53)$ GeV/n, $\Delta\gamma_O = 0.158 \pm 0.053$, with χ^2/d.o.f. = 3.0/8. The SPL fits gives $\gamma_C = -2.626 \pm 0.010$ with χ^2/d.o.f. = 27.5/10 for C, and $\gamma_O = -2.622 \pm 0.008$ with χ^2/d.o.f. = 15.9/10 for O, respectively. A frequentist test statistic $\Delta\chi^2$ is computed from the difference in χ^2 between the fits with SPL and DPL functions. For carbon (oxygen), $\Delta\chi^2 = 18.5(12.9)$ with 2 d.o.f. (i.e. the number of additional free parameters in DPL fit with respect to SPL fit) implies that the significance of the hardening of the C (O) spectrum exceeds the 3σ level. In order to study the energy dependence of the spectral index in a model independent way, the spectral index γ is calculated via a fit of $d[\log(\Phi)]/d[\log(E)]$ in energy windows centered in each bin and including the neighbor ±3 bins. The results in Fig. 3 show that carbon and oxygen fluxes harden in a similar way above a few hundred GeV/n. The carbon to oxygen flux ratio is well fitted to a constant value of 0.911 ± 0.006 above 25 GeV/n, confirming that the two fluxes have the same energy dependence [3].

4.2 The Boron spectrum and B/C ratio

The boron spectrum was published by CALET in [4]. It is reported in Fig. 4 as a function of kinetic energy per nucleon from 8.4 GeV/n to 3.8 TeV/n. Also, the carbon spectrum based on a larger dataset but consistent with our earlier result is shown. They are compared with results from

space-based [17, 25–28] and balloon-borne [22, 23, 29, 30] experiments. The boron spectrum is consistent with that of PAMELA [25]. The isotopic composition is assumed to be 70% of ^{11}B and 30% of ^{12}B.

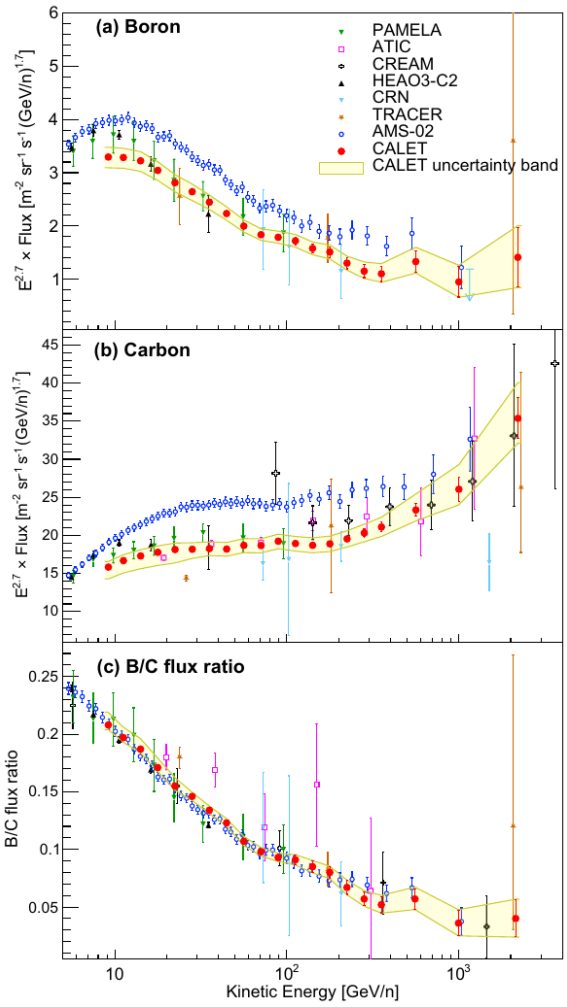

Figure 4: CALET (a) boron and (b) carbon flux (multiplied by $E^{2.7}$) and (c) ratio of boron to carbon, as a function of kinetic energy per nucleon E. Error bars of CALET data (red) represent the statistical uncertainty only, while the yellow band indicates the quadratic sum of statistical and systematic errors. Other direct measurements [17, 22, 25–31] are also plotted.

Different values of the ^{11}B abundance (±10%) cause a ∓1.7% difference in the boron spectrum. CALET result is well consistent with PAMELA, but lower than AMS-02 as in the cases of carbon, oxygen and iron spectra [3, 6]. The bottom panel of Fig. 4 shows the measurement of the B/C ratio as a function of kinetic energy per nucleon from 8.4 GeV/n to 3.8 TeV/n compared with the previous observations. CALET result is well consistent with previous measurements such as CREAM-I, PAMELA and AMS-02. The Fig. 5 shows the fits to CALET B and C data with a DPL. A SPL is also shown for comparison and the fit is limited to data points with 25 < E < 200 GeV/n and extrapolated above. The DPL fit to the C spectrum in the energy range [25, 3800] GeV/n yields $\gamma_C = -2.670 \pm 0.005$ and a spectral index increase $\Delta\gamma_C = 0.19 \pm 0.03$ at $E_0^C = (220 \pm 20)$ GeV/n confirming our first results reported in [3]. For the B spectrum, the parameter E_0^B is fixed to the fitted value of E_0^C. The best fit parameters for B are $\gamma_B = -3.047 \pm 0.024$ and $\Delta\gamma_B = 0.25 \pm 0.12$ with $\chi^2/\text{d.o.f} = 11.9/12$. The energy spectra are clearly different as expected for primary and secondary CRs, and the fit results seem to indicate, albeit with low statistical significance, that the flux hardens more for B than for C above 200 GeV/n. A similar indication also comes from the fit to the B/C flux ratio (Fig. 6). In the energy range [25, 3800] GeV/n, it can be fitted with a SPL function with spectral index $\Gamma = -0.366 \pm 0.018$ ($\chi^2/\text{d.o.f.} = 9.4/13$). Within the "leaky-box" (LB) approximate modeling of the particle transport in the Galaxy [30], the B/C flux ratio can be expressed as

$$\frac{\Phi_B(E)}{\Phi_C(E)} = \frac{\lambda(E)\lambda_B}{\lambda(E)+\lambda_B}\left[\frac{1}{\lambda_{C\to B}} + \frac{\Phi_O(E)}{\Phi_C(E)}\frac{1}{\lambda_{O\to B}}\right] \tag{4}$$

where λ_B is the interaction length of B nuclei with matter of the ISM and $\lambda_{C\to B}$ ($\lambda_{O\to B}$) is the average path length for a nucleus C (O) to spall into B. The LB model describes the diffusion of

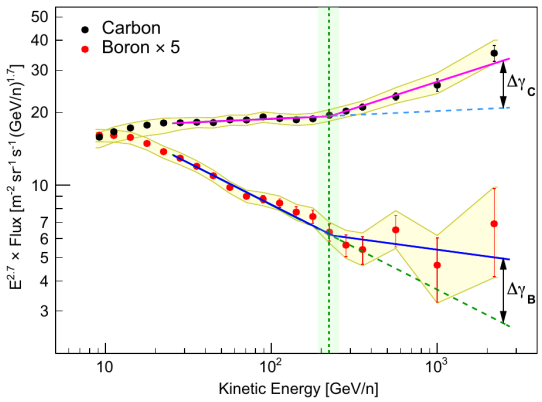

Figure 5: CALET B (red dots) and C (black dots) energy spectra are fitted with DPL functions (magenta line for C and blue line for (B) in the energy range [25, 3800] GeV/n. The B spectrum is multiplied by a factor 5 to overlap the low-energy region of the C spectrum. The dashed lines represent the extrapolation of a SPL function fitted to data in the energy range [25, 200] GeV/n. $\Delta\gamma$ is the change of the spectral index above the transition energy E_0^C (from the fit to C data), represented by the vertical green dashed line. The green band shows the error interval of E_0^C.

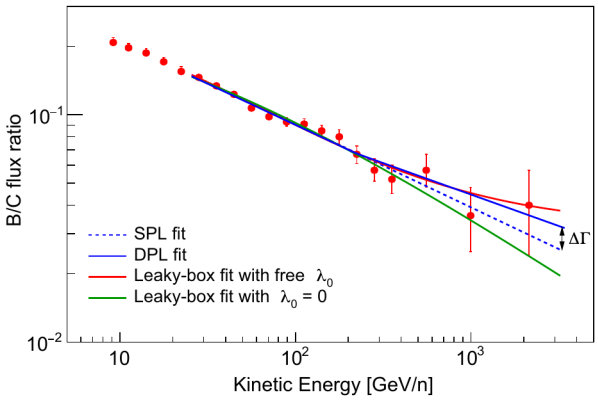

Figure 6: The CALET B/C ratio fitted to different functions. The error bars are the sum in quadrature of statistical and systematic uncertainties. The data are fitted to a DPL (solid blue line) and a SPL (dashed blue line) function in the energy interval [25, 3800] GeV/n. The red and green lines represent the fitted functions from a leaky-box model [Eq. 4] with the λ_0 parameter left free to vary and fixed to zero, respectively.

CRs in the Galaxy with a mean escape path length $\lambda(E)$ which, according to presently available direct measurements, is parametrized as a power-law function of kinetic energy E as follows:

$$\lambda(E) = kE^{-\delta} + \lambda_0 \tag{5}$$

where δ is the diffusion coefficient spectral index. A residual path length λ_0 is included in the asymptotic behavior of λ. Fitting our B/C data to Eq. 4 (Fig. 6), the best fit values without the source grammage term ($\lambda_0 = 0$) are $k = 11.2 \pm 0.5$ g/cm^2 and $\delta = 0.50 \pm 0.02$ (χ^2/d.o.f. = 13.6/13). Leaving instead λ_0 free to vary in the LB fit, we obtain $k = 12.0 \pm 0.9$ g/cm^2, $\delta = 0.71 \pm 0.11$, and $\lambda_0 = 0.95 \pm 0.35$ g/cm^2 (χ^2/d.o.f. = 9.6/12). These results suggest the possibility of a non-null value of the residual path length (though with a large uncertainty) which could be the cause of the apparent flattening of the B/C ratio at high energy.

4.3 The Iron flux

The spectrum of cosmic-ray iron was recently published by CALET [6]. The iron flux (multiplied by $E^{2.6}$) is shown in Fig. 7 (red filled circles) in the interval 10 GeV/n to 2.0 TeV/n. In comparison with other recent measurements, the CALET iron spectrum is consistent with ATIC02 [22] and TRACER [21] at low energy, and with CRN [18] and HESS [32] at high energy, while the absolute normalization is higher than NUCLEON [33] and lower than Sanriku [34]. AMS-02 [35] iron spectrum has a ~20% higher absolute normalization than CALET flux. However, when the latter is multiplied by $E^{2.7}$ (as in [35]) and normalized to the AMS-02 flux, the two spectra show

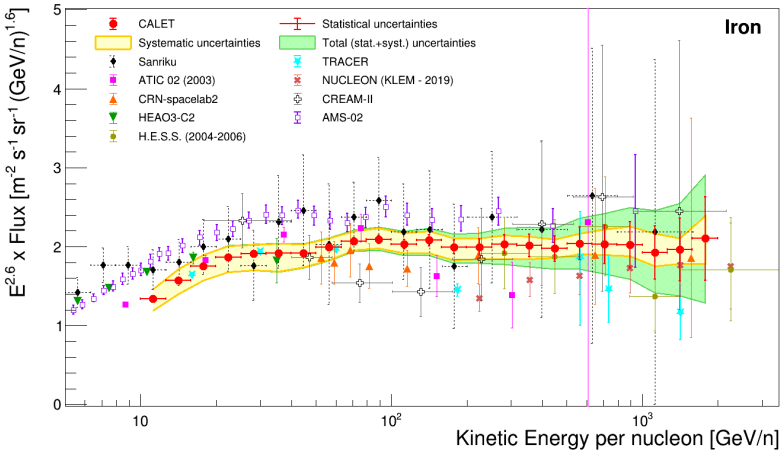

Figure 7: CALET iron flux (multiplied by E 2.6) as a function of kinetic energy per nucleon. Error bars of the CALET data (red) represent the statistical uncertainty only, the yellow band indicates the quadrature sum of systematic errors, while the green band indicates the quadrature sum of statistical and systematic errors. Other direct measurements [17, 18, 21, 22, 32–34] are also plotted.

a very similar shape and comparable errors (more details in the Supplemental Material of [6]). Fig. 8 shows a fit to a SPL function from 50 GeV/n to 2.0 TeV/n. The fit gives a spectral index $\gamma = -2.60 \pm 0.03$ with $\chi^2/\text{dof} = 4.2/14$. The result is stable when the binning is changed from 10 to 4 bins/decade ($\gamma = -2.59 \pm 0.04$). The energy dependence of the spectral index γ is also calculated by a fit of $\text{d}[\log(\Phi)]/\text{d}[\log(\text{E})]$ inside a sliding window centered in each energy bin and including the neighboring ±3 bins.

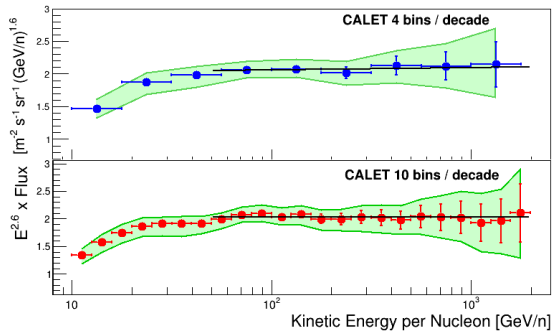

Figure 8: Fit of the CALET iron energy spectrum to a SPL function (black lines) in the energy range[50, 2000] GeV/n with 4 bins/decade (top) and 10 bins/decade (bottom). Both fluxes are multiplied by $\text{E}^{2.6}$ where E is the kinetic energy per nucleon. The error bars are representative of purely statistical errors whereas the green band indicates the quadrature sum of statistical and systematic errors.

The results in Fig. 8 show that the iron flux is compatible, within the errors, with a single power law in the fit region between 50 GeV/n and 2 TeV/n. The systematic error related to charge identification was studied by varying the semiaxes of the elliptical selection resulting in a flux variation lower than a few percent below 600 GeV/n. Using FLUKA (instead of EPICS [36]) as simulation code, the resulting fluxes show a maximum discrepancy around 10% below 40 GeV. The uncertainty on the energy scale correction is ±2% and causes a rigid shift of the measured energies, affecting the absolute flux normalization by $^{+3.3\%}_{-3.2\%}$, but not the spectral shape. The uncertainties due to the unfolding procedure were evaluated with different response matrices computed by varying the spectral index (between -2.9 and -2.2) of the MC generation spectrum, or by using the Singular Value Deconvolution method, instead of the Bayesian approach. The contributions due to the beam test model (not identical to the in-

strument now in orbit) and to the shower event cut were evaluated and included in the systematic uncertainties [6]. The systematic errors due to off-acceptance events, tracking efficiency, background contamination and HE trigger efficiency are negligible. Energy-independent systematic uncertainties affecting the flux normalization include live time (3.4%), long-term stability (< 2%), and geometrical factor (~1.6%).

4.4 The Nickel flux

The nickel spectrum was recently published by CALET in [7] and it is reported in Fig. 9 in the energy range from 8.8 GeV/n to 240 GeV/n where current uncertainties including statistical and systematic errors are bounded within a green band. The CALET spectrum is compared with

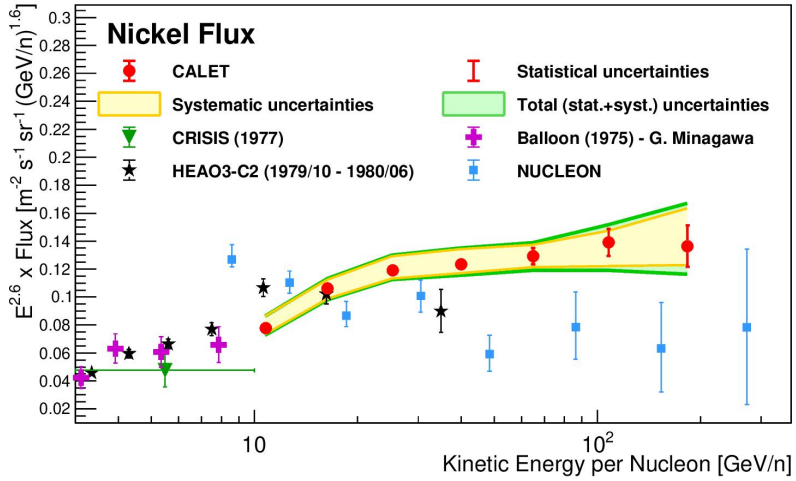

Figure 9: CALET nickel flux (multiplied by E 2.6) as a function of kinetic energy per nucleon. Error bars of the CALET data (red) represent the statistical uncertainty only, the yellow band in- dicates the quadrature sum of systematic errors, while the green band indicates the quadrature sum of statistical and systematic errors. The measurements from Balloon 1975 [37], CRISIS [38], HEAO3-C2 [17] and NUCLEON [39] are also plotted.

the results from Balloon 1975 [37], CRISIS [38], HEAO3-C2 [17], and NUCLEON [39]. CALET and HEAO3-C2 nickel spectra have similar flux normalization in the common interval of energies. CALET and NUCLEON differ in the shape although the two measurements show a similar flux normalization at low energy. The most important systematic uncertainties comprise the charge selection (different elliptical semi-axes give a flux variation lower than 4% at low energy increasing to ~8% at high energy), the MC model (using GEANT4 instead of EPICS we obtain a flux that differ by ~5% below 40 GeV/n and ~10% between 100 GeV/n and 200 GeV/n), the background contamination (between 1% below 100 GeV/n and 3% at 200 GeV/n) and the atomic mass of nickel isotope composition (that reduces the normalization by 2.2%). The other contributions considered also for the iron spectrum (energy scale, unfolding procedure, shower event selection, off-acceptance events, tracking, beam test configuration, long term stability, geometrical factor and live time) contribute up to a maximum of ~5% and are considered in the sum in quadrature of the total systematic uncertainty. The Fig. 10 shows a fit to the CALET nickel flux with a SPL. The fit is performed from 20 to 240 GeV/n and gives $\gamma = -2.51 \pm 0.07$ with a $\chi^2/\text{d.o.f} = 0.3/3$. Below

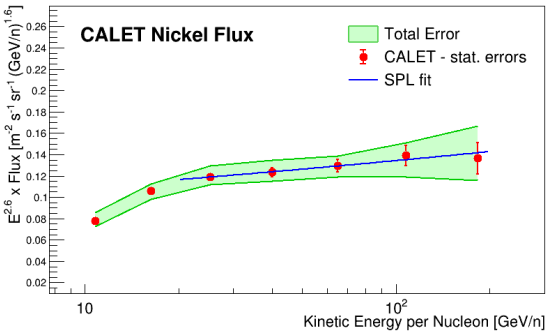

Figure 10: Fit of the CALET nickel energy spectrum to an SPL function (blue line) in the energy range [20, 240] GeV/n. The flux is multiplied by E 2.6 where E is the kinetic energy per nucleon. The error bars are representative of purely statistical errors.

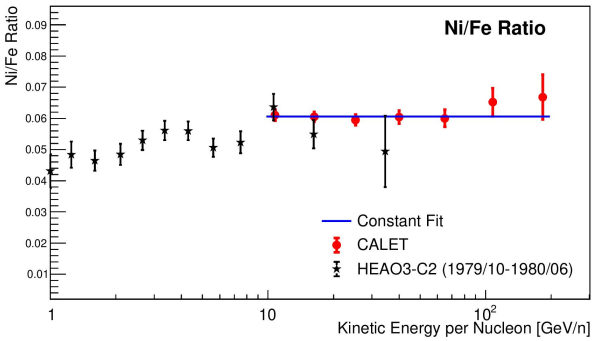

Figure 11: Nickel to iron flux ratio measured with CALET (red points). The errors bars are representative of statistical errors only. Data are fitted with a constant function giving Ni/Fe = 0.061 ± 0.001. Also plotted is the result from HEAO3-C2 [17].

20 GeV/n the observed Ni flux softening is similar to the one found for iron and lighter primaries. To better understand the nickel spectral behavior we report also the nickel to iron ratio as a function of kinetic energy per nucleon (see Fig. 11). Our measurement extends the results of previous experiments (i.e., HEAO3-C2) up to 240 GeV/n. The fit, performed from 8.8 to 240 GeV/n, gives a constant value of 0.061 ± 0.001 with the χ^2 = d.o.f. = 2.3/6. The experimental limitations of the present measurement (i.e., low statistics as well as large systematic errors for the highest energy bins) do not yet allow one to test the hypothesis of a spectral shape different from a single power law in the region above 20 GeV/n.

4.5 The Ultra Heavy Cosmic Rays

Ultra Heavy Cosmic Rays (UHCR) with charges $30 \leq Z \leq 40$ are $\sim 10^5$ less abundant than iron. In order to collect these rare events, CALET implements a special ultra-heavy trigger which provides an increased acceptance by requiring event trajectories to traverse the CHD and the top half of the IMC. This corresponds to an acceptance angle of ±75°, which gives an enhanced geometry factor of ~4400 $cm^2 sr$ (almost × 4 the total acceptance with the HE trigger). To date, single-element resolution measurements of UHCR have only been made by TIGER [40] (up to ^{40}Zr) and by SuperTIGER [41] (up to ^{56}Ba) balloon-borne instruments at GeV/n energies, as well by the ACE-CRIS [42] space based instrument (up to ^{40}Z) at lower energies (hundreds of MeV/n). The balloon based observations must be corrected for energy losses and nuclear interactions in the atmosphere, while ISS based measurements are subject to screening by the Earth's geomagnetic field. Comparatively, UHCR observations made by ACE-CRIS (sitting near the L1 libration point) occur outside the geomagnetic field and cover a complementary lower energy range. While ACE-CRIS and SuperTIGER instruments only measure charges down to B and Ne, respectively, CALET measures cosmic-ray abundances in the $1 \leq Z \leq 40$ charge range providing complementary measurements and a check of the cross calibrations of other instruments. Improved analyses of CALET UHCR, based on 5 years of data are reported in Figs. 12 and 13. The results shown are consistent with previous CALET findings [43] based on a smaller statistics, and are in good agreement with SuperTIGER. The lower energy interval covered by ACE-CRIS has to be taken

into account when comparing with CALET data. A preliminary comparison shows an approximate agreement.

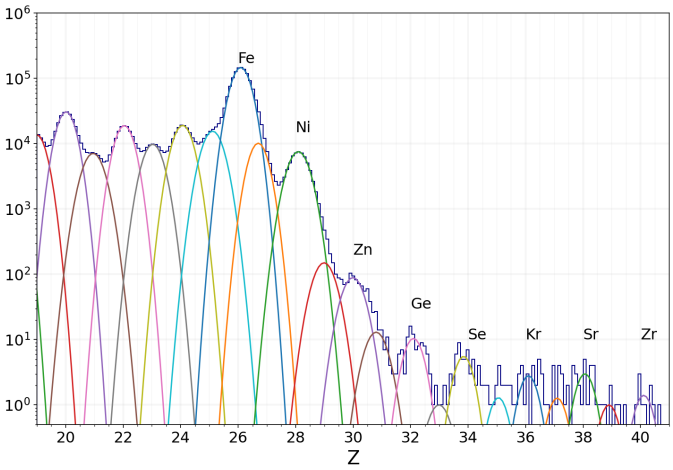

Figure 12: UHCR TASC analysis histogram with multiple Gaussian fitting, bin size in 0.1 units of charge.

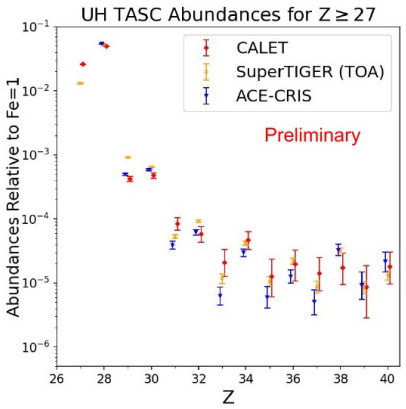

Figure 13: Comparison of the relative abundances measured by CALET with SuperTIGER [44] and ACE-CRIS [42] for Z between $27 \leq Z \leq 40$. Errors bars are statistical only.

5. Conclusions

The CALET space-based experiment installed on the International Space Station is collecting data smoothly since October 2015. At this workshop we presented the results published during the first seven years of operation. The carbon and oxygen spectra show a spectral hardening at several hundreds GeV/n excluding the hypothesis of a single power law by more than 3σ. Their ratio is compatible with a constant function in all the energy range with a value of 0.911 ± 0.001 confirming that they have the same energy dependence. The boron spectrum, recently published by CALET, shows a stronger hardening with respect to the carbon one above 200 GeV/n, as expected for primary and secondary cosmic rays. Their ratio can be fitted by a single power law with a spectral index $\Gamma = -0.366 \pm 0.018$. The interpretation through the leaky-box model was considered, suggesting the possibility of a non-null value of the residual path length which could explain the apparent flattening of the B/C ratio. The uncertainties given by the present statistics and large systematics of the iron spectrum do not allow us to draw a significant conclusion on a possible deviation from a single power law thus the spectrum above 50 GeV/n is compatible with a SPL with a spectral index $\gamma = -2.60 \pm 0.03$. The nickel spectrum, published by CALET extends the previous measurements up to 240 GeV/n with a better precision. The spectrum is compatible with a single power law with a spectral index $\gamma = -2.51 \pm 0.07$ in the energy range between 20 Gev/n and 240 GeV/n. The comparison of its behavior with respect to the iron spectrum shows that they have a similar energy dependence since their ratio is compatible with a constant function of value 0.061 ± 0.001. CALET provides also the relative abundances of elements more highly charged than nickel up to Z = 40,

thanks to a dedicated trigger mode that enhances the geometrical factor. These results, although preliminary, are very promising and will be published soon.

Acknowledgments

We gratefully acknowledge JAXA's contributions to the development of CALET and to the operations onboard the International Space Station. The CALET effort in Italy is supported by ASI ander Agreement No.2013-018-R.0 and its amendments. The CALET effort in the United States is supported by NASA through Grants No. 80NSSC20K0397, No. 80NSSC20K0399, and NNH18ZDA001N-APRA18-0004. This work is supported by JSPS KAKENHI Grant Numbers 19H05608 and 21K03592 in Japan.

DISCUSSION

Matteo Bachetti: There is often a discrepancy between the CALET spectra and the ones from previous experiments. How do you interpret this?

Caterina Checchia: The agreement between CALET and other experiments is generally good. However we have a discrepancy in fluxes normalization with AMS-02 although the shapes are very similar. The different normalization between the CALET and AMS-02 spectra (concerning carbon, oxygen, boron and iron) is still under study. We are investigating whether there are sources of systematic errors that have not been taken into account and the effect that different Monte Carlo simulations have on the fluxes.

References

[1] S. Torii and P.S. Marrocchesi, *The CALorimetric Electron Telescope (CALET) on the International Space Station*, *Advances in Space Research* **64** (2019) 2531.

[2] O. Adriani, Y. Akaike, K. Asano, Y. Asaoka, E. Berti, G. Bigongiari et al., *Observation of Spectral Structures in the Flux of Cosmic-Ray Protons from 50 GeV to 60 TeV with the Calorimetric Electron Telescope on the International Space Station*, *Phys. Rev. Lett.* **129** (2022) 101102.

[3] O. Adriani, Y. Akaike, K. Asano, Y. Asaoka, M.G. Bagliesi, E. Berti et al., *Direct Measurement of the Cosmic-Ray Carbon and Oxygen Spectra from 10 GeV/n to 2.2 TeV/n with the Calorimetric Electron Telescope on the International Space Station*, *Phys. Rev. Lett.* **125** (2020) 251102.

[4] O. Adriani, Y. Akaike, K. Asano, Y. Asaoka, E. Berti, G. Bigongiari et al., *Cosmic-Ray Boron Flux Measured from 8.4 GeV/n to 3.8 TeV/n with the Calorimetric Electron Telescope on the International Space Station*, *Phys. Rev. Lett.* **129** (2022) 251103.

[5] O. Adriani, Y. Akaike, K. Asano, Y. Asaoka, E. Berti, G. Bigongiari et al., *Direct Measurement of the Cosmic-Ray Helium Spectrum from 40 GeV to 250 TeV with the Calorimetric Electron Telescope on the International Space Station*, *Phys. Rev. Lett.* **130** (2023) 171002.

[6] O. Adriani, Y. Akaike, K. Asano, Y. Asaoka, E. Berti, G. Bigongiari et al., *Measurement of the Iron Spectrum in Cosmic Rays from 10 GeV/n to 2.0 TeV/n with the Calorimetric Electron Telescope on the International Space Station*, *Phys. Rev. Lett.* **126** (2021) 241101.

[7] O. Adriani, Y. Akaike, K. Asano, Y. Asaoka, E. Berti, G. Bigongiari et al., *Direct Measurement of the Nickel Spectrum in Cosmic Rays in the Energy Range from 8.8 GeV/n to 240 GeV/n with CALET on the International Space Station*, *Phys. Rev. Lett.* **128** (2022) 131103.

[8] W.V. Zober, B.F. Rauch, A. Ficklin and N.W. Cannady, *Progress on Ultra-Heavy Cosmic-Ray Analysis with CALET on the International Space Station*, *PoS* **ICRC2021** (2021) 124.

[9] S. Torii and Y. Asaoka, *Extended Measurement of Cosmic-Ray Electron and Positron Spectrum from CALET on the ISS*, *PoS* **ICRC2019** (2019) 142.

[10] P. Marrocchesi, O. Adriani, Y. Akaike, M. Bagliesi, A. Basti, G. Bigongiari et al., *Beam test performance of a scintillator-based detector for the charge identification of relativistic ions*, *Nuclear Instruments and Methods in Physics Research Section A: Accelerators, Spectrometers, Detectors and Associated Equipment* **659** (2011) 477.

[11] P. Brogi, P.S. Marrocchesi, P. Maestro and N. Mori, *CALET measurements with cosmic nuclei: expected performances of tracking and charge identification* , *PoS* **ICRC2015** (2016) 595.

[12] Y. Asaoka, Y. Akaike, Y. Komiya, R. Miyata, S. Torii, O. Adriani et al., *Energy calibration of CALET onboard the International Space Station*, *Astroparticle Physics* **91** (2017) 1.

[13] O. Adriani, Y. Akaike, K. Asano, Y. Asaoka, M.G. Bagliesi, G. Bigongiari et al., *Energy Spectrum of Cosmic-Ray Electron and Positron from 10 GeV to 3 TeV Observed with the Calorimetric Electron Telescope on the International Space Station*, *Phys. Rev. Lett.* **119** (2017) 181101.

[14] Y. Asaoka, *The CALorimetric Electron Telescope (CALET) on the International Space Station*, *PoS* **ICRC2019** (2019) 001.

[15] Y. Asaoka, S. Ozawa, S. Torii, O. Adriani, Y. Akaike, K. Asano et al., *On-orbit operations and offline data processing of CALET onboard the ISS*, *Astroparticle Physics* **100** (2018) 29.

[16] P. Maestro and N. Mori, *Particle tracking in the CALET experiment*, *PoS* **ICRC2017** (2017) 208.

[17] J.J. Engelmann, P. Ferrando, A. Soutoul, P. Goret, E. Juliusson, L. Koch-Miramond et al., *Charge composition and energy spectra of cosmic-ray nuclei for elements from Be to Ni - Results from HEAO-3-C2.*, *Astron. Astrophys.* **233** (1990) 96.

[18] D. Müeller, S.P. Swordy, P. Meyer, J. L'Heureux and J.M. Grunsfeld, *Energy Spectra and Composition of Primary Cosmic Rays*, *Astrophys. J.* **374** (1991) 356.

[19] E. Atkin, V. Bulatov, V. Dorokhov, N. Gorbunov, S. Filippov, V. Grebenyuk et al., *First results of the cosmic ray NUCLEON experiment*, *Journal of Cosmology and Astroparticle Physics* **2017** (2017) 020.

[20] M. Simon, H. Spiegelhauer, W.K.H. Schmidt, F. Siohan, J.F. Ormes, V.K. Balasubrahmanyan et al., *Energy spectra of cosmic-ray nuclei to above 100 GeV per nucleon*, *Astrophys. J.* **239** (1980) 712.

[21] M. Ave, P.J. Boyle, F. Gahbauer, C. Höppner, J.R. Hörandel, M. Ichimura et al., *Composition of Primary Cosmic-Ray Nuclei at High Energies*, *Astrophys. J.* **678** (2008) 262–273.

[22] A.D. Panov, J.H. Adams, H.S. Ahn et al., *Energy spectra of abundant nuclei of primary cosmic rays from the data of ATIC-2 experiment: Final results.*, *Bull. Russian Acad. Sci.* **73** (2009) 564.

[23] H.S. Ahn, P. Allison, M.G. Bagliesi, L. Barbier, J.J. Beatty, G. Bigongiari et al., *Energy spectra of cosmic-ray nuclei at high energies*, *The Astrophysical Journal* **707** (2009) 593.

[24] M. Aguilar, L. Ali Cavasonza, B. Alpat, G. Ambrosi, L. Arruda, N. Attig et al., *Observation of the Identical Rigidity Dependence of He, C, and O Cosmic Rays at High Rigidities by the Alpha Magnetic Spectrometer on the International Space Station*, *Phys. Rev. Lett.* **119** (2017) 251101.

[25] O. Adriani, G.C. Barbarino, G.A. Bazilevskaya, R. Bellotti, M. Boezio, E.A. Bogomolov et al., *Measurement of boron and carbon fluxes in cosmic rays with the PAMELA experiment*, *The Astrophysical Journal* **791** (2014) 93.

[26] S.P. Swordy, D. Mueller, P. Meyer, J. L'Heureux and J.M. Grunsfeld, *Relative Abundances of Secondary and Primary Cosmic Rays at High Energies*, *Astrophys. J.* **349** (1990) 625.

[27] M. Aguilar, L. Ali Cavasonza, G. Ambrosi, L. Arruda, N. Attig, S. Aupetit et al., *Observation of New Properties of Secondary Cosmic Rays Lithium, Beryllium, and Boron by the Alpha Magnetic Spectrometer on the International Space Station*, *Phys. Rev. Lett.* **120** (2018) 021101.

[28] M. Aguilar, L. Ali Cavasonza, G. Ambrosi, L. Arruda, N. Attig, F. Barao et al., *The Alpha Magnetic Spectrometer (AMS) on the international space station: Part II — Results from the first seven years*, *Physics Reports* **894** (2021) 1.

[29] H. Ahn, P. Allison, M. Bagliesi, J. Beatty, G. Bigongiari, P. Boyle et al., *Measurements of cosmic-ray secondary nuclei at high energies with the first flight of the CREAM balloon-borne experiment*, *Astroparticle Physics* **30** (2008) 133.

[30] A. Obermeier, P. Boyle, J. Hörandel and D. Müller, *The Boron-to-Carbon abundance ratio and galactic propagation of cosmic radiation*, *The Astrophysical Journal* **752** (2012) 69.

[31] Y.S. Yoon, H.S. Ahn, P.S. Allison, M.G. Bagliesi, J.J. Beatty, G. Bigongiari et al., *Cosmic-ray proton and helium spectra from the first CREAM flight*, *The Astrophysical Journal* **728** (2011) 122.

[32] F. Aharonian, A.G. Akhperjanian, A.R. Bazer-Bachi, M. Beilicke, W. Benbow, D. Berge et al., *First ground-based measurement of atmospheric Cherenkov light from cosmic rays*, *Phys. Rev. D* **75** (2007) 042004.

[33] V. Grebenyuk, D. Karmanov, I. Kovalev, I. Kudryashov, A. Kurganov, A. Panov et al., *Energy spectra of abundant cosmic-ray nuclei in the NUCLEON experiment*, *Advances in Space Research* **64** (2019) 2546.

[34] M. Ichimura, M. Kogawa, S. Kuramata, H. Mito, T. Murabayashi, H. Nanjo et al., *Observation of heavy cosmic-ray primaries over the wide energy range from ~100 GeV/particle to ~100 TeV/particle: Is the celebrated "knee" actually so prominent?*, *Phys. Rev. D* **48** (1993) 1949.

[35] M. Aguilar, L.A. Cavasonza, M.S. Allen, B. Alpat, G. Ambrosi, L. Arruda et al., *Properties of Iron Primary Cosmic Rays: Results from the Alpha Magnetic Spectrometer*, *Phys. Rev. Lett.* **126** (2021) 041104.

[36] See EPICS webpage `http://cosmos.n.kanagawa-u.ac.jp/EPICSHome/`.

[37] G. Minagawa, *The abundances and energy spectra of cosmic ray iron and nickel at energies from 1 to 10 GeV per AMU*, *Astrophys. J.* **248** (1981) 847.

[38] J.S. Young, P.S. Freier, C.J. Waddington, N.R. Brewster and R.K. Fickle, *The elemental and isotopic composition of cosmic rays - Silicon to nickel*, *Atrophys. J.* **246** (1981) 1014.

[39] V. Grebenyuk, D. Karmanov, I. Kovalev, I. Kudryashov, A. Kurganov, A. Panov et al., *Cosmic ray Nickel nuclei spectrum by the NUCLEON experiment*, 1809.07285.

[40] B.F. Rauch, J.T. Link, K. Lodders, M.H. Israel, L.M. Barbier, W.R. Binns et al., *Cosmic Ray Origin in OB Associations and Preferential Acceleration of Refractory Elements: Evidence from Abundances of Elements $_{26}Fe$ through $_{34}Fe$*, *The Astrophysical Journal* **697** (2009) 2083.

[41] R.P. Murphy, M. Sasaki, W.R. Binns, T.J. Brandt, T. Hams, M.H. Israel et al., *Galactic Cosmic Ray Origins and OB Associations: Evidence from SuperTIGER Observations of Elements $_{26}Fe$ through $_{40}Zr$*, *The Astrophysical Journal* **831** (2016) 148.

[42] W.R. Binns, M. Israel, M. Wiedenbeck, A.C. Cummings, R. Leske, R.A. Mewaldt et al., *Elemental Source Composition Measurements and the Origin of Galactic Cosmic Rays – ACE-CRIS Observations of UH Elements*, *PoS* **ICRC2019** (2019) 036.

[43] B.F. Rauch and W. Binns, *CALET Ultra Heavy Cosmic Ray Observations on the ISS*, *PoS* **ICRC2019** (2019) 130.

[44] N. Walsh, *Supertiger elemental abundances for the charge range $41 \leq z \leq 56$*, *Doctoral Dissertation* .

Full Author List: CALET Collaboration

O. Adriani[1,2], Y. Akaike[3,4], K. Asano[5], Y. Asaoka[5], E. Berti[2,6], G. Bigongiari[7,8], W.R. Binns[9], M. Bongi[1,2], P. Brogi[7,8], A. Bruno[10], N. Cannady[11,12,13], G. Castellini[6], C. Checchia[7,8], M.L. Cherry[14], G. Collazuol[15,16], G.A. de Nolfo[10], K. Ebisawa[17], A.W. Ficklin[14], H. Fuke[17], S. Gonzi[1,2,6], T.G. Guzik[14], T. Hams[11], K. Hibino[18], M. Ichimura[19], K. Ioka[20], W. Ishizaki[5], M.H. Israel[9], K. Kasahara[21], J. Kataoka[22], R. Kataoka[23], Y. Katayose[24], C. Kato[25], N. Kawanaka[20], Y. Kawakubo[14], K. Kobayashi[3,4], K. Kohri[26], H.S. Krawczynski[9], J.F. Krizmanic[12], P. Maestro[7,8], P.S. Marrocchesi[7,8], A.M. Messineo[8,27], J.W. Mitchell[12], S. Miyake[28], A.A. Moiseev[29,12,13], M. Mori[30], N. Mori[2], H.M. Motz[18], K. Munakata[25], S. Nakahira[17], J. Nishimura[17], S. Okuno[18], J.F. Ormes[31], S. Ozawa[32], L. Pacini[2,6], P. Papini[2], B.F. Rauch[9], S.B. Ricciarini[2,6], K. Sakai[11,12,13], T. Sakamoto[33], M. Sasaki[29,12,13], Y. Shimizu[18], A. Shiomi[34], P. Spillantini[1], F. Stolzi[7,8], S. Sugita[33], A. Sulaj[7,8], M. Takita[5], T. Tamura[18], T. Terasawa[5], S. Torii[3], Y. Tsunesada[35,36], Y. Uchihori[37], E. Vannuccini[2], J.P. Wefel[14], K. Yamaoka[38], S. Yanagita[39], A. Yoshida[33], K. Yoshida[21], and W.V. Zober[9]

[1]Department of Physics, University of Florence, Via Sansone, 1 - 50019, Sesto Fiorentino, Italy, [2]INFN Sezione di Firenze, Via Sansone, 1 - 50019, Sesto Fiorentino, Italy, [3]Waseda Research Institute for Science and Engineering, Waseda University, 17 Kikuicho, Shinjuku, Tokyo 162-0044, Japan, [4]JEM Utilization Center, Human Spaceflight Technology Directorate, Japan Aerospace Exploration Agency, 2-1-1 Sengen, Tsukuba, Ibaraki 305-8505, Japan, [5]Institute for Cosmic Ray Research, The University of Tokyo, 5-1-5 Kashiwa-no-Ha, Kashiwa, Chiba 277-8582, Japan, [6]Institute of Applied Physics (IFAC), National Research Council (CNR), Via Madonna del Piano, 10, 50019, Sesto Fiorentino, Italy, [7]Department of Physical Sciences, Earth and Environment, University of Siena, via Roma 56, 53100 Siena, Italy, [8]INFN Sezione di Pisa, Polo Fibonacci, Largo B. Pontecorvo, 3 - 56127 Pisa, Italy, [9]Department of Physics and McDonnell Center for the Space Sciences, Washington University, One Brookings Drive, St. Louis, Missouri 63130-4899, USA, [10]Heliospheric Physics Laboratory, NASA/GSFC, Greenbelt, Maryland 20771, USA, [11]Center for Space Sciences and Technology, University of Maryland, Baltimore County, 1000 Hilltop Circle, Baltimore, Maryland 21250, USA, [12]Astroparticle Physics Laboratory, NASA/GSFC, Greenbelt, Maryland 20771, USA, [13]Center for Research and Exploration in Space Sciences and Technology, NASA/GSFC, Greenbelt, Maryland 20771, USA, [14]Department of Physics and Astronomy, Louisiana State University, 202 Nicholson Hall, Baton Rouge, Louisiana 70803, USA, [15]Department of Physics and Astronomy, University of Padova, Via Marzolo, 8, 35131 Padova, Italy, [16]INFN Sezione di Padova, Via Marzolo, 8, 35131 Padova, Italy, [17]Institute of Space and Astronautical Science, Japan Aerospace Exploration Agency, 3-1-1 Yoshinodai, Chuo, Sagamihara, Kanagawa 252-5210, Japan, [18]Kanagawa University, 3-27-1 Rokkakubashi, Kanagawa, Yokohama, Kanagawa 221-8686, Japan, [19]Faculty of Science and Technology, Graduate School of Science and Technology, Hirosaki University, 3, Bunkyo, Hirosaki, Aomori 036-8561, Japan, [20]Yukawa Institute for Theoretical Physics, Kyoto University, Kitashirakawa Oiwake-cho, Sakyo-ku, Kyoto, 606-8502, Japan, [21]Department of Electronic Information Systems, Shibaura Institute of Technology, 307 Fukasaku, Minuma, Saitama 337-8570, Japan, [22]School of Advanced Science and Engineering, Waseda University, 3-4-1 Okubo, Shinjuku, Tokyo 169-8555, Japan, [23]National Institute of Polar Research, 10-3, Midori-cho, Tachikawa, Tokyo 190-8518, Japan, [24]Faculty of Engineering, Division of Intelligent Systems Engineering, Yokohama National University, 79-5 Tokiwadai, Hodogaya, Yokohama 240-8501, Japan, [25]Faculty of Science, Shinshu University, 3-1-1 Asahi, Matsumoto, Nagano 390-8621, Japan, [26]Institute of Particle and Nuclear Studies, High Energy Accelerator Research Organization, 1-1 Oho, Tsukuba, Ibaraki, 305-0801, Japan, [27]University of Pisa, Polo Fibonacci, Largo B. Pontecorvo, 3 - 56127 Pisa, Italy, [28]Department of Electrical and Electronic Systems Engineering, National Institute of Technology (KOSEN), Ibaraki College, 866 Nakane, Hitachinaka, Ibaraki 312-8508, Japan, [29]Department of Astronomy, University of Maryland, College Park, Maryland 20742, USA, [30]Department of Physical Sciences, College of Science and Engineering, Ritsumeikan University, Shiga 525-8577, Japan, [31]Department of Physics and Astronomy, University of Denver, Physics Building, Room 211, 2112 East Wesley Avenue, Denver, Colorado 80208-6900, USA, [32]Quantum ICT Advanced Development Center, National Institute of Information and Communications Technology, 4-2-1 Nukui-Kitamachi, Koganei, Tokyo 184-8795, Japan, [33]College of Science and Engineering, Department of Physics and Mathematics, Aoyama Gakuin University, 5-10-1 Fuchinobe, Chuo, Sagamihara, Kanagawa 252-5258, Japan, [34]College of Industrial Technology, Nihon University, 1-2-1 Izumi, Narashino, Chiba 275-8575, Japan, [35]Graduate School of Science, Osaka Metropolitan University, Sugimoto, Sumiyoshi, Osaka 558-8585, Japan, [36]Nambu Yoichiro Institute for Theoretical and Experimental Physics, Osaka Metropolitan University, Sugimoto, Sumiyoshi, Osaka 558-8585, Japan, [37]National Institutes for Quantum and Radiation Science and Technology, 4-9-1 Anagawa, Inage, Chiba 263-8555, Japan, [38]Nagoya University, Furo, Chikusa, Nagoya 464-8601, Japan, [39]College of Science, Ibaraki University, 2-1-1 Bunkyo, Mito, Ibaraki 310-8512, Japan

PoS(MULTIF2023)011